Journal of The Electrochemical Society, **157** (9) B1269-B1274 (2010)
0013-4651/2010/157(9)/B1269/6/$28.00 © The Electrochemical Society

Nanopore Patterned Pt Array Electrodes for Triple Phase Boundary Study in Low Temperature SOFC

Young Beom Kim,[a,*,z] Ching-Mei Hsu,[b] Steve T. Connor,[c] Turgut M. Gür,[b,] Yi Cui,[b,**] and Fritz B. Prinz[a,b,**]**

[a]*Department of Mechanical Engineering,* [b]*Department of Material Science and Engineering, and* [c]*Department of Chemistry, Stanford University, Stanford, California 94305, USA*

This paper describes the fabrication and investigation of morphologically stable model electrode structures with well-defined and sharp platinum/yttria-stabilized zirconia (YSZ) interfaces to study geometric effects at triple phase boundaries (TPBs). A nanosphere patterning technique using monodispersed silica nanoparticles, which are applied to the YSZ surface by the Langmuir–Blodgett method, is employed to deposit nonporous platinum electrodes containing close-packed arrays of circular openings 300–400 nm in diameter through which the underlying YSZ surface is exposed to the gas phase. These nanostructured dense Pt array cathodes exhibited better structural integrity and thermal stability at the solid oxide fuel cell (SOFC) operating temperature of 450–500°C when compared to porous sputtered Pt electrodes. More importantly, electrochemical studies on geometrically well-defined Pt/YSZ sharp interfaces demonstrated that the cathode impedance and cell performance both scale almost linearly with the aerial density of TPB length. These controlled experiments also demonstrated that when normalized with respect to TPB length, the performance of different cells with different TBP densities agree well each other, indicating that TPB length governs cell performance especially in the activation polarization regime, as expected. Cells with a higher TPB density achieved better fuel cell performance in terms of higher power density and lower electrode impedance.
 [DOI: 10.1149/1.3455046]

Manuscript submitted January 25, 2010; revised manuscript received April 21, 2010. Published July 9, 2010. This was Paper 1466 presented at the Vienna, Austria, Meeting of the Society, October 4–9, 2009.

Solid oxide fuel cells (SOFCs) are efficient energy conversion devices that are being developed for practical applications. Due to large activation energies (~1 eV) for oxide ion transport in solid oxide electrolytes and relatively sluggish oxygen reduction reaction at the cathode, SOFCs are usually operated at elevated temperatures (800–1000°C) to obtain practically meaningful fluxes and fuel cell performance. Typically, an SOFC element is made of an yttria-stabilized zirconia (YSZ) electrolyte layer, a mixed conducting ceramic cathode such as $La_{1-x}Sr_xCo_{1-y}Fe_yO_3$ (LSCF) and $La_{1-x}Sr_xMnO_{3-\delta}$ (LSM), and a cermet anode such as Ni/YSZ.

The operation of SOFCs at elevated temperatures may be desirable for enhanced kinetics and transport purposes but poses serious challenges in microstructural and thermal stability, seal integrity, aging and degradation, thermal cycling, and cost of materials and fabrication. To mitigate some of these problems, recent efforts have been aimed toward lowering the operating temperature of SOFCs to an intermediate temperature (IT) regime of 600–800°C, i.e., IT-SOFCs.[1-4] Although oxygen chemical diffusion in mixed conducting electrodes such as LSCF and LSM is relatively fast at elevated temperatures,[5-9] their catalytic activities and transport rates decrease precipitously with temperature that leads to increased activation losses at ITs.[1,10-13]

In recent years, the thrust of our research effort has been aimed to further lower the operating temperature of SOFCs to a regime between 300 and 500°C by employing thin-film structures of the YSZ electrolyte and electrodes.[14-17] As expected, the use of mixed conducting ceramic cathodes for such low temperature (LT) (300–500°C) SOFCs would not be meaningful due to severe losses expected from large overpotentials at the electrodes. Hence, platinum is selected as a model electrode material in this study not only to enhance the fuel cell performance but also to provide a stable and geometrically well-defined platform to examine the triple phase boundary (TPB) effects in SOFCs. In this relatively LT regime, Pt remains to be the best catalyst to enhance the rate for the oxygen reduction reaction at the cathode that is critically important to minimize the activation loss and to improve the fuel cell performance of LT-SOFCs.

The primary purpose of this paper is to control the geometry of the Pt/YSZ interface that makes it possible to investigate TPB effects in a quantifiable manner. Although similar patterning efforts have been reported, only a handful has considered the Pt/YSZ system,[18,19] while most were intended for mixed oxide cathodes such as La–Sr–Mn–O.[20,21]

The methodology developed in this study allowed the fabrication of morphologically stable Pt array electrodes that exhibit sharp and well-defined TPBs. The strategy was to define the geometry of the three-phase contact interfaces while providing a dense and nonporous Pt layer that constrains the charge-transfer reaction to TPB only as well as eliminating porosity effects at the Pt/YSZ interface under the Pt layer. This patterning approach opens up the opportunity for other researchers to systematically study TPB effects in SOFCs. The results presented here successfully demonstrate that controlled TPB density correlates well with cell performance.

The charge-transfer reaction at the cathode involves the reduction of oxygen at the TPB, where the gas, catalytic cathode, and electrolyte are all in physical contact. Due to the relatively high activation energy of >1.5 eV for the oxygen reduction reaction,[22-27] it is generally agreed that the processes at the cathode govern the overall behavior of SOFCs even at elevated temperatures.[1] Naturally, cathodic overvoltage becomes even more pronounced at the low operating temperatures employed in this study. To mitigate this effect and to enhance fuel cell performance, it is desirable not only to maximize the TPB density but also to employ a Pt catalyst at the cathode to improve the reaction kinetics for oxygen reduction in LT-SOFCs. However, improved performance was not the focal point of this study.

Typically, dc sputtering is employed to deposit porous Pt electrodes that increase TPB density for improved fuel cell performance. However, this technique poses challenges to quantify the TPB geometry and to carry out systematic studies of TPB effects in SOFCs because control, quantification, and stability of the Pt/YSZ interface morphology are not trivial issues. It is difficult to characterize the morphological details of the Pt/YSZ interface with sufficient precision.[1,28-30] Also, time-dependent changes,[31] such as the Ostwald ripening of the sputtered porous Pt electrodes that can lead to microstructural coarsening and degradation, complicate the problem furthermore. Indeed, recent work in our laboratory has shown that sputtered porous pure Pt electrodes are not thermally stable even at the low operating temperatures of LT-SOFCs.[32] Most importantly,

* Electrochemical Society Student Member.
** Electrochemical Society Active Member.
z E-mail: ybkim@stanford.edu

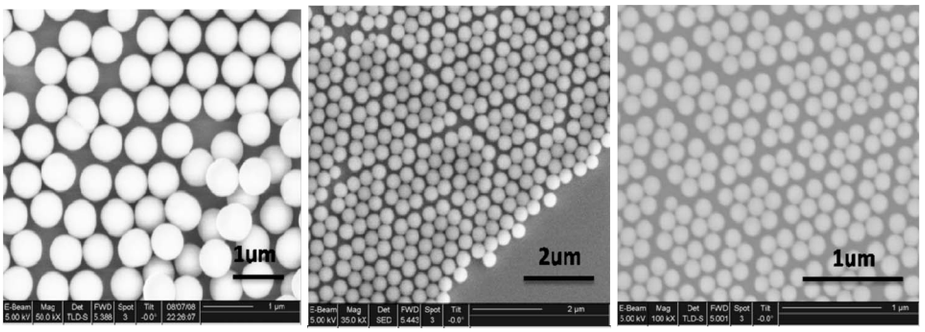

Figure 1. Synthesized spherical silica particles with different diameters: 700 (left), 300 (center), and 150 nm (right).

however, it is difficult to quantify and define the exact geometry, scale, and nanostructure of the TPB. This makes the quantitative investigation of the rate processes at the TPB challenging.

It is for these reasons that the present paper reports on a nonlithographic patterning technique for fabrication of dense Pt electrodes with easily tunable and well-defined TPB geometry. The intent is not to achieve improved cell performance but, rather, to establish a methodology that allows a systematic investigation of TPB characteristic and scaling behavior.

This paper presents a dense patterned Pt architecture that forms sharp, stable Pt/YSZ interfaces with well-defined geometries, and hence, allows determination of TPB linear density with good accuracy. Because the Pt electrode layer is nonporous, this architecture also restricts the charge-transfer reaction to this geometrically defined interface. Furthermore, the present paper demonstrates superior microstructural and thermal stability of such patterned electrodes for improved and consistent SOFC performance. The nanosphere patterning method provides the ability to vary the TPB geometry, which makes it possible to investigate TPB characteristics in a controlled manner. This paper is a prelude to an ongoing work in our laboratory for the quantitative study and characterization of the TPB and its scaling behavior.

Experimental

The fabrication of nanopore patterned dense Pt electrodes was conducted on the cathode side of the SOFC. Initially, a masking solution was created from monosized spherical silica particles by a modified Stöber synthesis technique using tetraethyl orthosilicate (TEOS).[33-35] The TEOS molecules were easily converted to silicon dioxide via a series of condensation reactions. Initially, pH $\sim$ 12 was employed in a mixture of ammonium hydroxide and ethanol as a basic catalyst. The rate of conversion was sensitive to the presence of either an acidic or basic catalyst. The size of the spherical silica particles was controlled by varying the concentration of TEOS and the catalyst. Thus, different sizes of nanospherical silica particles were prepared and used as mask for the subsequent patterning of the Pt cathode layers (Fig. 1).

Monosized spherical silica particles were transferred onto a surface of the YSZ substrate using a Langmuir–Blodgett (LB) trough technique developed by Hsu and co-workers.[36] Initially, the LB trough was filled with deionized water. Then the prepared silica particles were introduced onto the surface of the water by slow injection. Using the compression bars in the trough, a monolayer of nanospherical particles was produced at the surface. The substrate was then dipped into the trough and pulled out at a constant rate. In this case, the substrate is a 1×1 cm and 100 μm thick 8% YSZ polycrystalline wafer obtained from Marketech Inc. The transfer process involved the slow insertion of the YSZ substrate vertically into the LB trough and removing the adhered spherical particles as a film from the liquid surface by steadily withdrawing the YSZ substrate from the liquid at a finite rate. This method created a close-packed monolayer of silica particles on the YSZ substrate. By appropriately varying the silica particle size and the spacing between particles, it was possible to vary and optimize the TPB density on the YSZ surface in a controlled manner. For this study, two initially different sizes of nanospherical particles were employed, namely 450 and 330 nm, to make nanopore structured Pt electrodes with different TPB densities.

After forming a close-packed monolayer of spherical particles on the substrate, anisotropic plasma etching was used to uniformly reduce the size of the silica particles to open up space between them for depositing Pt through the interspacing between the particles. A dense Pt layer was then deposited on the cathode side by dc sputtering under 100 W of plasma power and 1 Pa of Ar pressure for about 60 s at room temperature. This yielded a nonporous Pt film of about 60 nm in thickness.[16] Then the silica particles were removed mechanically from the YSZ substrate using ultrasonication. On the anode side of the substrate, an 80 nm thick porous Pt layer was deposited by dc sputtering under 50 W of power and 10 Pa of Ar pressure for 150 s at room temperature. With that, the fabrication of the SOFC membrane electrode assembly (MEA) was completed. This process yielded a patterned Pt cathode layer with well-defined geometry that enabled the study of TPB geometric effects in a systematic and controlled manner (Fig. 2).

For the fuel cell performance characterization, we used a homemade experimental chamber with a micromanipulating probe station (Fig. 3). During the measurements, pure dry hydrogen was provided at the anode side as fuel and air was used as the oxygen source at the cathode side. Constant temperature was maintained by a temperature controlling unit. For electrochemical characterization, a Gamry potentiostat (Gamry Instruments) unit was used for collecting both the current–voltage (*I-V*) characteristic data and electrochemical impedance spectra (EIS) in the frequency range of 30 kHz–0.1 Hz with an ac amplitude of 50 mV.

Results and Discussion

SOFCs that operate at elevated temperatures typically do not employ Pt electrodes. However, for LT-SOFCs, the use of Pt electrodes is a near necessity due to the sluggish reaction kinetics at these LTs. Micro-SOFCs utilizing 50–750 nm thick YSZ membranes and porous Pt electrodes have been studied, and power densities in the range 0.02–152 mW/cm^2 have been reported.[37] Comparatively, a similar work in our laboratory has demonstrated record power densities of up to 861 mW/cm^2 at 450°C.[14-16] The long-term stability of the sputtered Pt electrodes reported in these studies, however, has not been fully documented or investigated. Similarly, there is no coherent understanding or established process for the consistent fabrication of stable Pt electrode morphologies that also display optimum performance. Previously, evidence from our laboratory has indicated that porous Pt electrodes fabricated by dc sputtering undergo morphological changes during cell operation even at these LTs, while stable morphology and performance were demonstrated with Pt–Ni alloy electrodes.[32] Based on these observations, dense Pt electrodes with geometric openings to create well-defined and stable TPB were pursued in the present study.

The sharp interfacial geometry of the open pores in a close-packed fashion makes it possible to approximate the TPB density (cm/cm^2) for a given patterned area. With the help of scanning

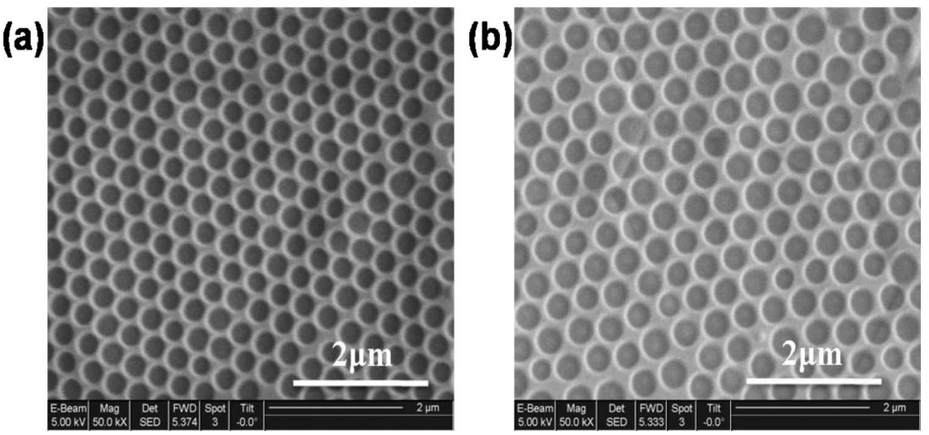

Figure 2. Nanopore structured dense Pt electrode with different final pore sizes and TPB density: (a) 300 and (b) 400 nm. SEM images were taken with the same magnification, and the image with smaller initial particle size shows denser pores, which relates to increased TPB density.

electron microscopy (SEM) images, the TPB densities for the two patterned Pt cathodes were approximated to be 8.93×10^4 cm/cm^2 for cathodes with a 300 nm opening and 5.07×10^4 cm/cm^2 for cathodes with a 400 nm opening. The SOFC MEA with the smaller initial diameter of the silica particle showed about a factor of 1.8 higher TPB density than the SOFC MEA with the larger size of the starting silica particles. Naturally, the size of the pore opening as well as the interspacing between openings for a given geometric area determine the TPB density. The results presented below correlate the TPB scaling factor with cell performance and behavior.

Although the fuel cell MEA with porous Pt electrodes outperformed that with patterned Pt cathode at the beginning of cell testing, its performance dramatically decreased within a short time due to electrode degradation. The change in the morphology of the dc-sputtered porous Pt electrodes before and after fuel cell testing at elevated temperature is shown in Fig. 4a and b. Even at the moderately low (400–450°C) operating temperature of LT-SOFC, significant changes clearly take place in the microstructure of the porous Pt electrode driven likely by its high surface energy. However, due to the visibly evident changes in the Pt morphology and equally so at the Pt/YSZ interface, the reduction in the TPB density leads to a rapid degradation in the fuel cell performance until it seems to stabilize at a significantly lower value. This is shown in Fig. 5, which compares the fuel cell performance of sputtered porous Pt electrodes with patterned Pt electrodes under potentiostatic conditions. After the completion of the *I-V* experiments for both samples, the output currents of the two cells were monitored for 12 h at 500°C at a constant voltage that corresponds to the peak power density value. Despite the noise in the data that came from the measurement setup, particularly from the on/off-type temperature controller and the fume hood fan, Fig. 5 clearly indicates a stable performance of the nanostructured Pt electrode, while the current output from the porous Pt cell clearly shows a rapid decay over time. In addition, a morphological comparison provided in Fig. 6 demonstrates the stability of the nanostructured Pt electrode after running under potentiostatic conditions for 12 h at 500°C. This morphological degradation occurs even at a temperature lower than 500°C and becomes observable within a short period of time. Unlike the porous Pt cathodes, the patterned Pt morphology indicated no discernible change in the microstructure at the test temperatures and under load in an SOFC configuration. Clearly, the sharp interfacial edges of the Pt layer, representing the location of TPB, are uniformly well preserved even after prolonged use. The results demonstrate that the nanopatterning method employed in this study helped stabilize the morphology and provide thermal and microstructural stability at fuel cell operating temperatures.

Furthermore, nanopatterned Pt electrodes, when optimized, have

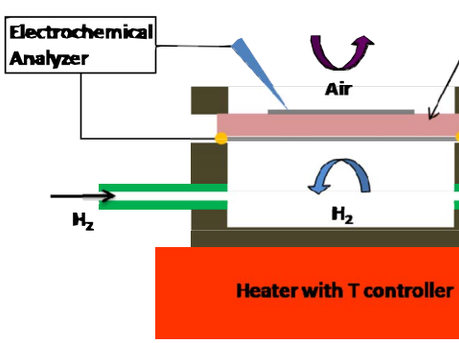

Figure 3. (Color online) Schematic illustration of the probing station for electrochemical characterization of fuel cell MEAs.

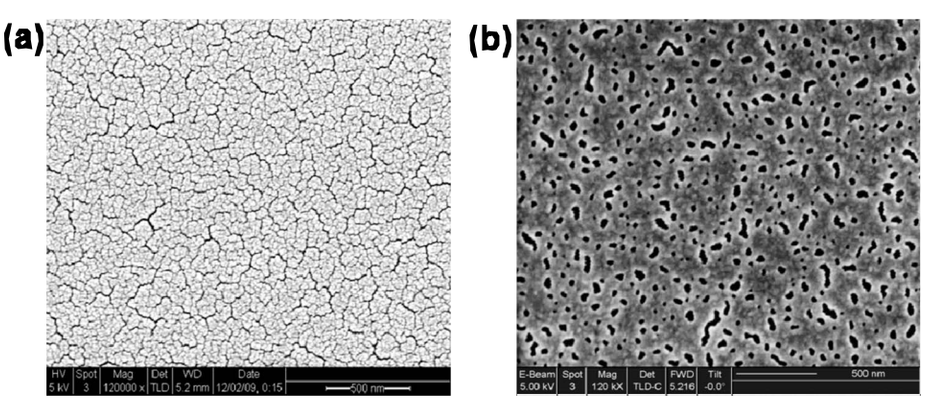

Figure 4. SEM images of (a) as-sputtered porous Pt layer and (b) after a short time (~30 min) operation of fuel cell at elevated temperature (450°C), clearly indicating a dramatic change in Pt morphology and a proportionate reduction in the TPB density.

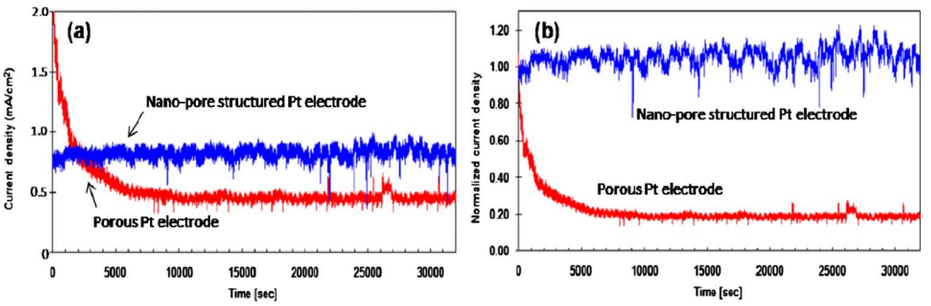

Figure 5. (Color online) Potentioamperometry data at 0.6 V, comparing the behavior of SOFC MEA with porous Pt electrode and SOFC with nanopore structured Pt electrode. Measurement was conducted for 12 h continuously at 500°C. (a) Absolute output current densities indicating severe degradation in performance of porous Pt within a short time as opposed to stable behavior of patterned dense Pt. (b) Normalized current density plot showing relative amounts of degradation from the initial performance.

the potential to provide better cell performance due to controlled and stable TPB geometries that also offer ready access to the gas phase. Indeed, this is demonstrated in Fig. 7, which compares the performance of an SOFC MEA at 450°C featuring a nanopatterned Pt electrode of approximately 400 nm diameter pore size with that of a MEA with dc-sputtered porous Pt electrodes measured after the cell performance is stabilized at the operating temperature. The cell featuring nanopatterned Pt clearly performs better than the one having a porous sputtered Pt electrode. This result suggests either a higher density of TPB for the nanopatterned Pt electrode or possibly a significant amount of closed porosity in the sputtered Pt electrode that is likely due to structural coarsening and degradation, which hinders direct access from the gas phase, even though it might have initially possessed a larger Pt/YSZ interfacial contact length. The maximum power density values obtained with fuel cell MEAs with nanopatterned cathodes are still orders of magnitude lower than those of previous papers from our laboratory on record performance of LT-SOCFs using a thin-film YSZ electrolyte and a porous Pt electrode.[14-16] This is primarily due to two reasons, namely that the TPB density of nanopatterned cathodes is naturally and significantly lower than porous Pt cathodes, and that polycrystalline 100 μm thick bulk YSZ wafers were used as the electrolyte in the present study. Therefore, it may not be meaningful to directly compare these performance values due to the combined effect of the electrolyte thickness and deposition methods, which generate different microstructures. Again, this paper presents a fabrication methodology for nanopore structured electrodes not for the purpose of achieving higher performance but for investigation of the electrochemical behavior of TPB geometry and possibly its optimization.

The performance of fuel cells featuring two different nanopore sizes, or respective TPB densities, is presented in Fig. 8a. The SOFC MEA with a higher density TPB of about 8.93×10^4 cm/cm^2 of projected area (pore diameter of ~300 nm) at the cathode shows better performance than the SOFC with coarser (~400 nm) cathode openings with a TPB density of about 5.07×10^4 cm/cm^2. These values are larger than the 15–150 m/cm^2 TPB densities reported for patterned Pt electrodes on YSZ.[19] The peak power densities and open-circuit voltages of the patterned Pt cathodes with pore openings of 300 and 400 nm pore size are 2.2 mW/cm^2 and 1.04 V and 1.4 mW/cm^2 and 1.01 V at 450°C, respectively, at about a cell operating voltage of 0.45 V. Also, the coarser TPB sample shows a larger exponential drop at a low current region, indicative of a larger activation loss than the denser TPB sample. However, the differences in their relative performances vanish when these plots are normalized with respect to the areal TPB densities of the two MEAs.

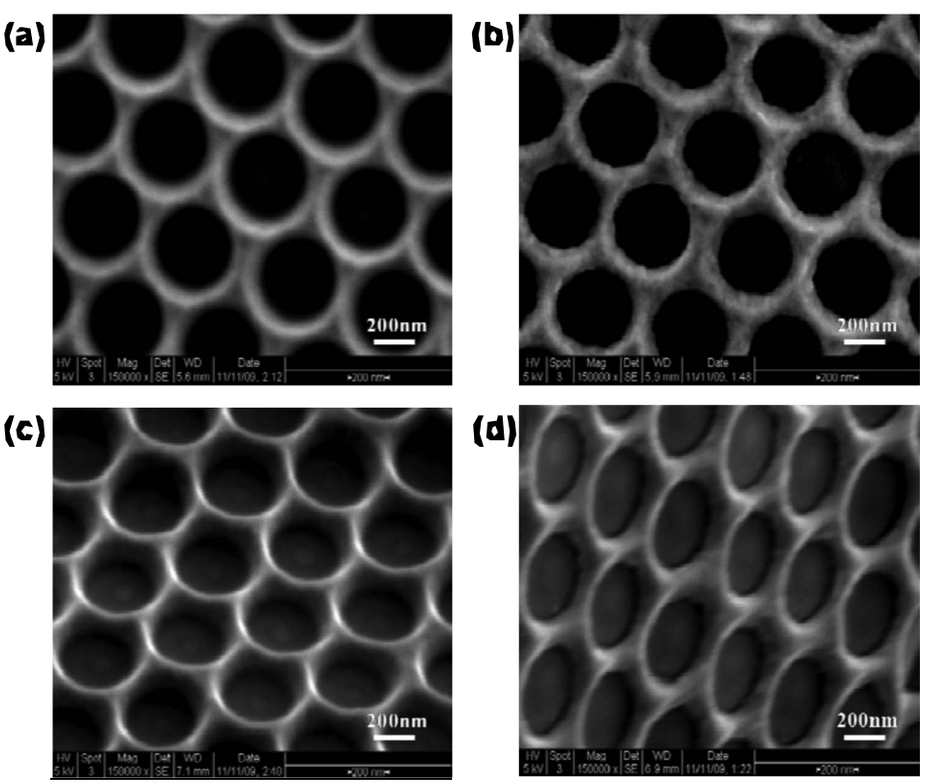

Figure 6. High resolution SEM images of nanostructured fresh Pt electrode [(a) top and (c) tilted views] before running and [(b) top and (d) tilted views] after running chronoamperometrically for 12 h at 500°C. Clearly, nanostructured Pt does not show any major morphological change, and the TPBs are well conserved after long operation.

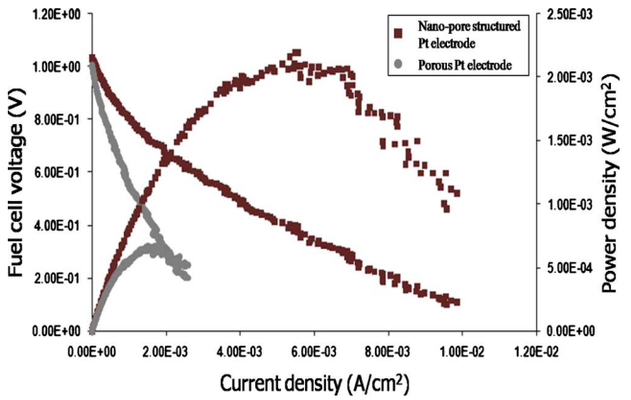

Figure 7. (Color online) *I-V-P* comparison of SOFC at 450°C employing dc sputtered porous Pt electrode vs nanopore structured Pt electrode at the cathode.

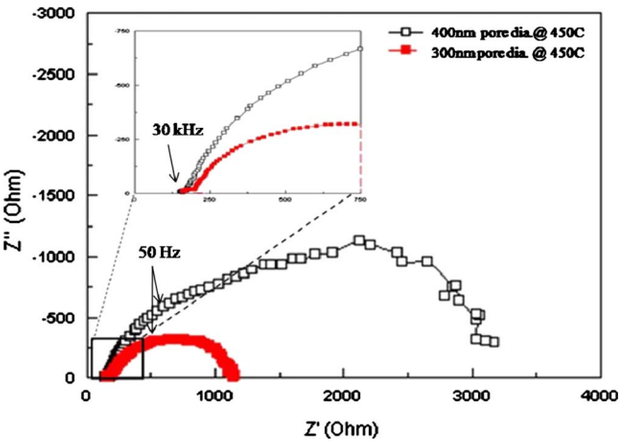

Figure 9. (Color online) EIS Nyquist spectra of SOFC samples featuring nanopore structured dense Pt cathodes with different TPB densities.

This is expected because the charge-transfer reaction is restricted to the TPB whose linear length per unit area is determined by the masking process during patterning. The results are shown in Fig. 8b, where the *I-V-P* plots of the 300 and 400 nm patterned MEAs overlap on top of each other in an almost perfect registry and agreement on the low current regime, where activation losses and, hence, the charge transfer along TPB dominate the behavior.

Further characterization of the MEAs was carried out by EIS. Figure 9 compares the EIS spectra at 450°C of SOFC samples with nanopatterned Pt cathodes of different pore opening sizes under 0.6 V dc biased condition. From the EIS Nyquist plot of the SOFC with a YSZ electrolyte, the high frequency arc corresponds to the ohmic resistance of the electrolyte and the low frequency arc corresponds to the electrochemical reaction at the electrolyte/electrode interface.[33] For SOFCs, there is a general agreement that cathode reaction kinetics is much slower than that for the anode reaction, and hence, the cathode reaction dominates the activation loss.[3] By assigning the low frequency arc in the EIS spectra to the oxygen reduction reaction process as suggested by others,[38,39] one can conclude that the cathode impedance is reduced for the 300 nm pore size Pt electrode due to increased TPB density as compared to the 400 nm pore size Pt having a lower TPB density, and hence, a larger cathode impedance. Clearly, the EIS impedance data provide further support for faster or improved oxygen reduction kinetics at the cathode by increasing the TPB density and the charge-transfer reaction sites.[40]

From the EIS spectra in Fig. 9, it is possible to determine the corresponding cathode resistance for the two samples. The electrode resistance of the coarser TPB MEA (~2600 Ω) is a factor of 2.06 higher than the MEA with a denser TPB (~1260 Ω), corresponding to smaller pore openings. Although the scaling factor does not perfectly match the ratio of 1.8 between the TPB densities of the two samples, it does suggest within experimental error that the electrode resistance scales almost linearly with the TPB density.

Furthermore, a similar scaling behavior is observed between the TPB density and the peak power densities of the two samples shown in the *I-V* curves of Fig. 8. Indeed, the ratio of 1.6 between the peak power densities of the two samples agrees within experimental error with the TPB ratio of 1.8 between the two patterned cathode samples, suggesting again the possibility of a linear scaling law.

Considering that the linear length of the Pt/YSZ interface per circular opening in these patterned cathodes is about 1260 nm for the 400 nm diameter opening, and correspondingly 940 nm for the 300 nm diameter opening, the results above further suggest that the TPB width under the test conditions is significantly smaller than its length, possibly in the several nanometers to tens of nanometers range in general agreement with estimated literature values of the same order of magnitude.[18] This yields a near-linear scaling relationship.

Work is in progress at our laboratory along this direction. We are pursuing fabrication of dense Pt cathode layers with increasingly smaller opening diameters perhaps down to 50 nm or less to study their scaling behavior. The expectation is to observe the transition of the linear scaling law into an areal scaling behavior at sufficiently small openings where the TPB widths overlap and cover the entire exposed YSZ area in the cathode opening. This line of investigation is expected to provide further understanding regarding the TPB geometry and behavior, and achieve further enhancement in fuel cell performance by increasing and tuning the TPB density by advanced patterning tools and methods.

Conclusion

The present study offers a process methodology for controlling the geometry of the Pt/YSZ interface for the systematic study of TPB characteristics. The results presented here point to several important and useful consequences. First is the near-linear scaling law of cell impedance and, correspondingly, cell performance on the

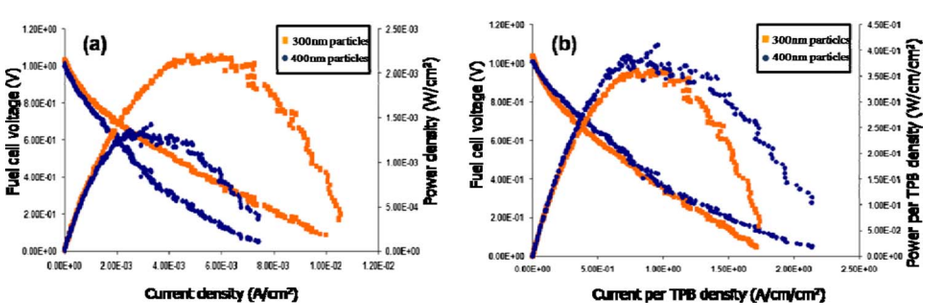

Figure 8. (Color online) (a) Fuel cell *I-V* measurement of SOFC samples at 450°C with structured electrode with different pore diameters. (b) *I-V-P* plot where current is normalized by TPB density. The plots overlap in good registry especially in the activation regime as expected and indicate that fuel cell performance scales with TPB density.

linear density of TPB. The EIS spectra showed significant improvement in the oxygen reduction kinetics with increased TPB density. The linear scaling behavior infers that the charge-transfer reaction is constrained to TPB as expected. It also implies that the width of TPB in our MEAs is negligibly small with respect to its length, which agrees with literature. Second is the precision and versatility of the patterning method presented here to fabricate dense electrodes with sharp interfaces and well-defined geometries. These electrodes also exhibit superior stability compared to sputtered Pt electrodes and maintain their morphology and microstructure intact after prolonged fuel cell operation. Third is the opportunity of stable operation of IT to LT SOFCs that employ these dense and patterned electrodes. Fourth is the ability to study TPB geometric effects in a controllable and reproducible manner over a wide range of circular pore diameters using this powerful patterning technique that does not require lithography and micromachining. The pore size and TPB density are easily tunable by changing the initial size of the masking silica particles and the spacing between them. Studies to further understand and determine TPB geometry at the Pt/YSZ interface and optimize the TPB density are currently underway in our laboratory.

Acknowledgments

S.T.C. acknowledges the support of an NSF Graduate Fellowship.

Stanford University assisted in meeting the publication costs of this article.

References

1. J. Fleig, *Annu. Rev. Mater. Res.*, **33**, 361 (2003).
2. Y. Jiang and A. V. Virkar, *J. Electrochem. Soc.*, **150**, A942 (2003).
3. S. de Souza, S. J. Visco, and L. C. De Jonghe, *Solid State Ionics*, **98**, 57 (1997).
4. E. D. Wacshman, *ECS Trans.*, **25**(2), 783 (2009).
5. A. Belzner, T. M. Gür, and R. A. Huggins, *Solid State Ionics*, **57**, 327 (1992).
6. K. Nisancioglu and T. M. Gür, *Solid State Ionics*, **72**, 199 (1994).
7. S. Sunde, K. Nisancioglu, and T. M. Gür, *J. Electrochem. Soc.*, **143**, 3497 (1996).
8. S. Diethelm, A. Closset, K. Nisancioglu, J. Van herle, A. J. McEvoy, and T. M. Gür, *J. Electrochem. Soc.*, **146**, 2606 (1999).
9. R. Doshi, J. L. Routbort, and C. B. Alcock, *Defect Diffus. Forum*, **127–128**, 39 (1995).
10. S. B. Adler, *Chem. Rev. (Washington, D.C.)*, **104**, 4791 (2004).
11. S. Wang, T. Kato, S. Nagata, T. Kaneko, N. Iwashita, T. Honda, and M. Dokiya, *Solid State Ionics*, **152–153**, 477 (2002).
12. B. C. H. Steele, *Solid State Ionics*, **134**, 3 (2000).
13. R. Doshi, V. L. Richards, J. D. Carter, X. Wang, and M. Krumpelt, *J. Electrochem. Soc.*, **146**, 1273 (1999).
14. P.-C. Su, C.-C. Chao, J. H. Shim, R. Fasching, and F. B. Prinz, *Nano Lett.*, **8**, 2289 (2008).
15. J. H. Shim, C.-C. Chao, H. Huang, and F. B. Prinz, *Chem. Mater.*, **19**, 3850 (2007).
16. H. Huang, M. Nakamura, P. Su, R. Fasching, Y. Saito, and F. B. Prinz, *J. Electrochem. Soc.*, **154**, B20 (2007).
17. H. Huang, T. M. Gür, Y. Saito, and F. Prinz, *Appl. Phys. Lett.*, **89**, 143107 (2006).
18. J. L. Hertz and H. L. Tuller, *Solid State Ionics*, **178**, 915 (2007).
19. A. Mitterdorfer and L. J. Gauckler, *Solid State Ionics*, **117**, 203 (1999).
20. R. Radhakrishnan, A. V. Virkar, and S. C. Singhal, *J. Electrochem. Soc.*, **152**, A210 (2005).
21. V. Brichzin, J. Fleig, H.-U. Habermeier, and J. Maier, *Electrochem. Solid-State Lett.*, **3**, 403 (2000).
22. E. Siebert, A. Hammouche, and M. Kleitz, *Electrochim. Acta*, **40**, 1741 (1995).
23. B. C. H. Steele, *Solid State Ionics*, **86–88**, 1223 (1996).
24. J. Van Herle, A. J. McEvoy, and K. R. Thampi, *Electrochim. Acta*, **41**, 1447 (1996).
25. A. Mitterdorfer and L. J. Gauckler, *Solid State Ionics*, **111**, 185 (1998).
26. Y. Matsuzaki and I. Yasuda, *Solid State Ionics*, **126**, 307 (1999).
27. M. Juhl, S. Primdahl, C. Manon, and M. Mogensen, *J. Power Sources*, **61**, 173 (1996).
28. E. Mutoro, S. Günther, B. Luerssen, I. Valov, and J. Janek, *Solid State Ionics*, **179**, 1835 (2008).
29. E. Mutoro, B. Luerssen, S. Günther, and J. Janek, *Solid State Ionics*, **179**, 1214 (2008).
30. F. S. Baumann, J. Fleig, H.-U. Habermeier, and J. Maier, *Solid State Ionics*, **177**, 1071 (2006).
31. T. M. Gür and R. A. Huggins, *J. Appl. Electrochem.*, **17**, 800 (1987).
32. X. Wang, H. Huang, T. Holme, X. Tian, and F. B. Prinz, *J. Power Sources*, **175**, 75 (2008).
33. G. H. Bogush, M. A. Tracy, and C. F. Zukoski IV, *J. Non-Cryst. Solids*, **104**, 95 (1988).
34. W. Stöber, A. Fink, and E. Bohn, *J. Colloid Interface Sci.*, **26**, 62 (1968).
35. G. H. Bogush and C. F. Zukoski IV, *J. Colloid Interface Sci.*, **142**, 1 (1991).
36. C.-M. Hsu, S. T. Connor, M. X. Tang, and Y. Cui, *Appl. Phys. Lett.*, **93**, 133109 (2008).
37. A. Evans, A. Bieberle-Hütter, J. L. M. Rupp, and L. J. Gauckler, *J. Power Sources*, **194**, 119 (2009).
38. E. Barsoukov and J. R. Macdonald, *Impedance Spectroscopy: Theory, Experiment, and Applications*, 2nd ed., John Wiley & Sons, New York (2005).
39. H. Huang, T. Holme, and F. B. Prinz, *ECS Trans.*, **3**(32), 31 (2007).
40. A. Optiz, A. Schintlmeister, H. Hutter, and J. Fleig, *ECS Trans.*, **25**(2), 2783 (2009).